AIP | Journal of Applied Physics

Strain and piezoelectric potential effects on optical properties in CdSe/CdS core/shell quantum dots

Seoung-Hwan Park and Yong-Hoon Cho

Citation: J. Appl. Phys. **109**, 113103 (2011); doi: 10.1063/1.3594743
View online: http://dx.doi.org/10.1063/1.3594743
View Table of Contents: http://jap.aip.org/resource/1/JAPIAU/v109/i11
Published by the American Institute of Physics.

Strain and piezoelectric potential effects on optical properties in CdSe/CdS core/shell quantum dots

Seoung-Hwan Park[1] and Yong-Hoon Cho[2]
[1]*Department of Electronics Engineering, Catholic University of Daegu, Hayang, Kyeongbuk 712-702, Republic of Korea*
[2]*Department of Physics, Graduate School of Nanoscience and Technology (WCU), and KI for the NanoCentury, KAIST, Daejeon 305-701, Republic of Korea*

(Received 4 March 2011; accepted 27 April 2011; published online 3 June 2011)

Strain and piezoelectric potential effects on optical properties in CdSe/CdS core/shell quantum dots (QDs) were investigated theoretically using an eight-band strain-dependent $\mathbf{k}\cdot\mathbf{p}$ Hamiltonian. The strain effect on the shift of the subband energies is found to be larger than the piezoelectric field effect. As a result, interband transition energies are blueshifted with the inclusion of strain and piezoelectric field effects. We know that the theoretical interband transition energy shows a reasonable agreement with the experimental result. The absolute value of the hydrostatic strain in the QD increases with decreasing QD size, whereas that in the barrier decreases with decreasing QD size. © *2011 American Institute of Physics*. [doi:10.1063/1.3594743]

I. INTRODUCTION

Quantum dots (QDs) are interesting because their electronic and optical properties dramatically change as the size of the quantum dot varies.[1] Currently, III–V materials are the leading ones for the fabrication of QDs. On the other hand, recently, the II–VI materials have been studied by numerous workers due to their large bandgap and their potential applications in short-wavelength optoelectronic devices.[2–4] Among them, CdSe/CdS core/shell nanoparticles have attracted a lot of attention in the past decade because they have great stability and a high fluorescence quantum yield. The wurtzite CdSe/CdS core/shell QDs are usually synthesized by wet chemical routes such as the microemulsion method followed by refluxing in toluene/methanol.[5,6] In the wurtzite structure, the strain-induced piezoelectric potential arises due to strain-induced lattice distortions. The detailed knowledge of the internal potential and the strain field in and around the QDs can serve as a useful tool to understand their electronic and optical properties. Despite their importance, however, there have been very little theoretical works on strain and piezoelectric potential effects on optical properties of core/shell CdSe/CdS QDs are still not well understood.

In this paper, strain and piezoelectric potential effects on optical properties in CdSe/CdS core/shell QDs are investigated theoretically using an eight-band strain-dependent $\mathbf{k}\cdot\mathbf{p}$ Hamiltonian. The wurtzite CdSe/CdS core/shell nanocrystal fabricated by wet chemical routes is known to have a type I structure,[6] although a type II structure was found in the case of certain quantum well structures grown by metal-organic chemical vapor deposition or hot wall beam epitaxy.[7,8] Here, we assumed that the CdSe/CdS system yields a type I interface. The potential offsets between the core and shell are approximated by the differences between the bulk electron affinities and ionization potentials of CdSe and CdS.[9] The 8×8 Hamiltonian is solved by using a three-dimensional finite-element method (FEM) formulation.[10,11]

II. THEORY

The energy levels and wave functions of bound electron and hole states are calculated in the frame of the eight-band $\mathbf{k}\cdot\mathbf{p}$ model. The effective-mass Hamiltonian H_w in the presence of strain is given by[12]

$$H_w=\begin{pmatrix} A_c & 0 & V & 0 & -V^* & 0 & U & 0 \\ 0 & A_c & 0 & V & 0 & -V^* & 0 & U \\ V^* & 0 & F & -K^* & -H^* & 0 & 0 & 0 \\ 0 & V^* & -K & G & H & 0 & 0 & \Delta \\ -V & 0 & -H & H^* & \lambda & 0 & \Delta & 0 \\ 0 & -V & 0 & 0 & 0 & F & -K & H \\ U^* & 0 & 0 & 0 & \Delta & -K^* & G & -H^* \\ 0 & U^* & 0 & \Delta & 0 & H^* & -H & \lambda \end{pmatrix}\begin{matrix}|1\rangle\\|2\rangle\\|3\rangle\\|4\rangle\\|5\rangle\\|6\rangle\\|7\rangle\\|8\rangle\end{matrix} \tag{2.1}$$

where

$$\begin{aligned}
A_c &= E_g+\frac{\hbar^2}{2m_c^*}\left(k_x^2+k_y^2+k_z^2\right)+a_c^t\left(\varepsilon_{xx}+\varepsilon_{yy}\right)+a_c^z\varepsilon_{zz}+V_c,\\
V &= -\frac{P_2}{\sqrt{2}}\left(k_x+ik_y\right)+\frac{P_2}{\sqrt{2}}\sum_j\left(\varepsilon_{xj}+i\varepsilon_{yj}\right)k_j,\\
U &= P_1k_z-P_1\sum_j\varepsilon_{zj}k_j,\\
F &= \Delta_1+\Delta_2+\lambda+\theta,\\
G &= \Delta_1-\Delta_2+\lambda+\theta,\\
\lambda &= \frac{\hbar^2}{2m_0}\left[A_1k_z^2+A_2\left(k_x^2+k_y^2\right)\right]+\lambda_\varepsilon+V_h,\\
\theta &= \frac{\hbar^2}{2m_0}\left[A_3k_z^2+A_4\left(k_x^2+k_y^2\right)\right]+\theta_\varepsilon,\\
K &= \frac{\hbar^2}{2m_0}A_5\left(k_x+ik_y\right)^2+D_5\varepsilon_+,\\
H &= \frac{\hbar^2}{2m_0}A_6\left(k_x+ik_y\right)k_z+D_6\varepsilon_{z+},\\
\lambda_\varepsilon &= D_1\varepsilon_{zz}+D_2\left(\varepsilon_{xx}+\varepsilon_{yy}\right),\\
\theta_\varepsilon &= D_3\varepsilon_{zz}+D_4\left(\varepsilon_{xx}+\varepsilon_{yy}\right),\\
\Delta &= \sqrt{2}\Delta_3,\\
\varepsilon_\pm &= \varepsilon_{xx}\pm 2i\varepsilon_{xy}-\varepsilon_{yy},\\
\varepsilon_{z\pm} &= \varepsilon_{zx}\pm i\varepsilon_{yz}.
\end{aligned} \tag{2.2}$$

Here, P_1 and P_2 are the conduction band transverse (longitudinal) deformation potentials. The A_i's are the valence-band effective-mass parameters, which are similar to the Luttinger parameters in a zinc-blende crystal, the D_i's are the deformation potentials for wurtzite crystals, k_i is the wave vector, ε_{ij} is the strain tensor, Δ_1 is the crystal-field split energy, and Δ_2 and Δ_3 account for spin–orbit interactions. Zhang[13] pointed out that strain gradient terms are important when the strain is not sufficiently small and its variation is not sufficiently slow. In the present model, strain gradient terms were neglected as the first approximation. The basis set for a wurtzite crystal is summarized as follows:

$$
\begin{aligned}
|1\rangle &= |iS\rangle \uparrow \\
|2\rangle &= |iS\rangle \downarrow \\
|3\rangle &= -\frac{1}{\sqrt{2}}[|X\rangle + i|Y\rangle] \uparrow \\
|4\rangle &= \frac{1}{\sqrt{2}}[|X\rangle - i|Y\rangle] \uparrow \\
|5\rangle &= |Z\rangle \uparrow \\
|6\rangle &= \frac{1}{\sqrt{2}}[|X\rangle - i|Y\rangle] \downarrow \\
|7\rangle &= -\frac{1}{\sqrt{2}}[|X\rangle + i|Y\rangle] \downarrow \\
|8\rangle &= |Z\rangle \downarrow .
\end{aligned} \tag{2.3}
$$

The electron potential $V_e(x,y,z)$ and the hole potential $V_h(x,y,z)$ are defined as

$$
V_c(x,y,z) = \begin{cases} 0 & \text{insidedot} \\ V_{e0} & \text{others} \end{cases} \tag{2.4}
$$

and

$$
V_h(x,y,z) = \begin{cases} 0 & \text{insidedot} \\ V_{h0} & \text{others.} \end{cases} \tag{2.5}
$$

The energies and the envelope functions of the conduction and the valence subbands can be obtained by solving the effective-mass equation

$$
\begin{aligned}
&\sum_{\nu} H_{\mu\nu} F_{\nu}(x,y,z) = E F_{\mu}(x,y,z), \\
&\nu,\mu \in \{|1\rangle,|2\rangle,|3\rangle,|4\rangle,|5\rangle,|6\rangle,|7\rangle,|8\rangle\},
\end{aligned} \tag{2.6}
$$

where H is the Luttinger-Khon 8×8 Hamiltonian. According to the theory of linear elasticity, the stress–strain relationship for linear conditions, including initial stress and strain, is given as

$$
\sigma_{ij} = C_{ijlm}\left[\varepsilon_{lm} - (\varepsilon_0)_{lm}\right], \qquad i,j,l,m = x,y,z, \tag{2.7}
$$

where C_{ijlm} is the component of the fourth-order elastic moduli tensor. The elastic strain was calculated using the theory of continuum elasticity and FEM.[10,11] The strain-induced piezoelectric polarization is given by

$$
P_i = e_{ijk}\varepsilon_{jk}. \tag{2.8}
$$

Symmetry considerations allow 27 constants for e_{ijk} to be reduced to just three independent components for the wurtzite structures, which for convenience are renamed: $e_{15} = e_{113} = e_{223}$, $e_{31} = e_{311} = e_{322}$, and $e_{33} = e_{333}$. Thus, the total polarization is given by

$$
\mathbf{P} = \begin{pmatrix} 2e_{15}\varepsilon_{13} \\ 2e_{15}\varepsilon_{23} \\ e_{31}(\varepsilon_{11}+\varepsilon_{22}) + e_{33}\varepsilon_{33} \end{pmatrix}. \tag{2.9}
$$

The piezoelectric potential ϕ is obtained from the Poisson equation

$$
\varepsilon_0 \nabla \cdot (\varepsilon_r \nabla \phi) = -\nabla \cdot \mathbf{P} \tag{2.10}
$$

where ε_0 and ε_r are the dielectric constant in vacuum and the relative static dielectric tensor, respectively. The material parameters for CdSe and CdS used in the computations were give in Table I.

TABLE I. Physical parameters used in the calculation.

Parameters	CdSe	CdS
Lattice constant (Å)		
a[a]	4.3	4.136
Energy parameter (eV)		
(E_g)[a]	1.98	2.58
(Δ_1)[b]	0.039	0.027
$(\Delta_2 = \Delta_3)$[b]	0.416	0.065
Valence band effective-mass parameters[b]		
A_1	− 5.06	− 4.53
A_2	− 0.43	− 0.39
A_3	2.58	3.84
A_4	− 1.29	− 1.92
A_5	0.89[c]	1.33[c]
A_6	− 0.65[c]	0.93[c]
Deformation potentials[d] (eV)		
(a_c^t)	− 7.8	− 8.2
(a_c^z)	− 1.76	− 4.5
D_1	− 0.76	− 2.8
D_2	− 3.7	− 4.5
D_5	1.2	0.58
Elastic stiffness constant[e] (10^{11} dyn/cm^2)		
C_{11}	7.41	9.07
C_{12}	4.52	5.81
C_{13}	3.93	5.10
C_{33}	8.36	9.38
C_{44}	1.317	1.504
Dielectric constant(ε_0)[f]		
(ε)	9.29	8.28
Piezoelectric constant (C/m^2)		
(e_{15})	− 0.138[g]	− 0.21[e]
(e_{13})	− 0.16[g]	− 0.24[e]
(e_{33})	0.347[g]	0.44[e]

[a]Reference 14.
[b]Reference 15.
[c]This work.
[d]Reference 16.
[e]Reference 17.
[f]Reference 18.
[g]Reference 19.

III. RESULTS AND DISCUSSION

Figure 1 shows (a) potential by the strain-induced piezoelectric polarization along the z-axis and (b) ground-state subband energies in the conduction and the valence bands as a function of the diameter of the CdSe QD for strained CdSe/CdS core/shell QD structures. For comparison, we plotted results for subband energies without piezoelectric polarization effect. The internal field is determined from the difference between piezoelectric fields in the QD and that in the barrier. Thus, the strain-induced potential depends on the structural parameter such as the QD size. The potential is shown to be at a maximum near the boundary between the QD region and the barrier region. On the other hand, it becomes zero near the QD center. The subband energies gradually decrease due to the quantization effect with increasing QD size. We know that subband energies in the conduction and the valence bands are shifted downward with the inclusion of the piezoelectric field. However, the piezoelectric field effect on the subband energy is relatively very small for QDs with small QD size.

Figure 2 shows strain tensors of the CdSe QD for strained CdSe/CdS core/shell QD structures with several QD diameters. Here, the thickness of the CdS shell is fixed to be 7 Å. The CdSe core is assumed to be initially unstrained because CdS shell is grown on the CdSe core. On the other hand, the misfit strain of the CdS shell is taken with respect to the CdS core and so the QD is assumed to be strained initially by ε_{xx0} $(=\varepsilon_{yy0})$ and ε_{zz0} as a qualitative approximation. The initial strain is taken as positive for a material under tensile strain and their value for the present system are $\varepsilon_{xx0}=3.96$ and $\varepsilon_{zz0}=4.60\%$, respectively. The strain was calculated by using the theory of linear elasticity.[20,21] In the QD, ε_{xx} is shown to be nearly the same as ε_{yy} irrespectively of the QD size. This biaxial compressive strain occurs due to the surrounding material forcing the CdSe QD to have the lattice constant of CdS. This is accompanied by an extension, indicated by a peak of ε_{zz} near the boundary between the QD and the barrier. That is, ε_{zz} becomes tensile in the surrounding matrix because the QD exerts the opposite force on the surrounding matrix.

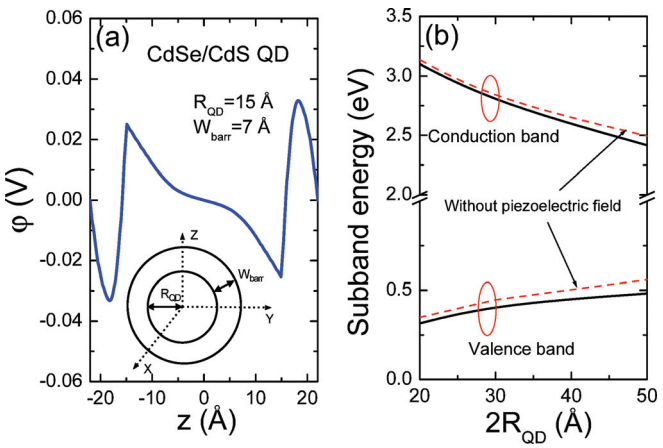

FIG. 1. (Color online) (a) Potential by the strain-induced piezoelectric polarization along the z-axis and (b) ground-state subband energies in the conduction and the valence bands as a function of the diameter of the CdSe QD for strained CdSe/CdS core/shell QD structures. For comparison, we plotted results for subband energies without piezoelectric polarization effect.

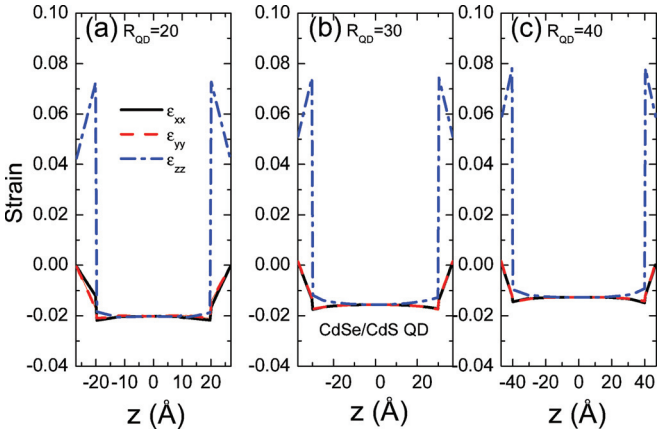

FIG. 2. (Color online) Strain tensors of the CdSe QD for strained CdSe/CdS core/shell QD structures with several QD diameters. Here, the thickness of the CdS shell is fixed to be 7 Å.

Figure 3 shows hydrostatic strain along the z-direction through the center of the CdSe QD for strained CdSe/CdS core/shell QD structures with several QD diameters. Here, the thickness of the CdS shell is fixed to be 7 Å. The hydrostatic strain is given by the sum of the three normal components $\varepsilon_h=\varepsilon_{xx}+\varepsilon_{yy}+\varepsilon_{zz}$, which is related to the shift of the conduction and the valence band energy levels, respectively. The hydrostatic strain is compressive in the QD and tensile in the barrier. The hydrostatic strain changes sign from negative to positive at the QD/matrix interface. The absolute value of the hydrostatic strain in the QD increases with decreasing QD size. For example, absolute values of the hydrostatic strain at $z=0$ are 8.4 and 5.7% for QDs with $R_{QD}=20$ and 50 Å, respectively. On the other hand, the absolute value of the hydrostatic strain in the barrier decreases with decreasing QD size.

Figure 4 shows (a) ground-state subband energies in the conduction and the valence bands and (b) interband transition energies as a function of the diameter of the CdSe QD for strained CdSe/CdS core/shell QD structures and comparison with experimental data. The experimental data for the CdSe/CdS core/shell QD structure was taken from Ref. 6 For comparison, we plotted results for subband energies without

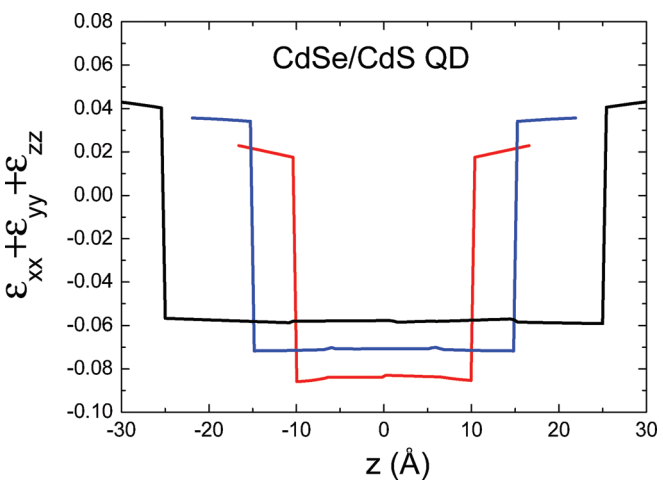

FIG. 3. (Color online) Hydrostatic strain along the z-direction through the center of the CdSe QD for strained CdSe/CdS core/shell QD structures with several QD diameters.

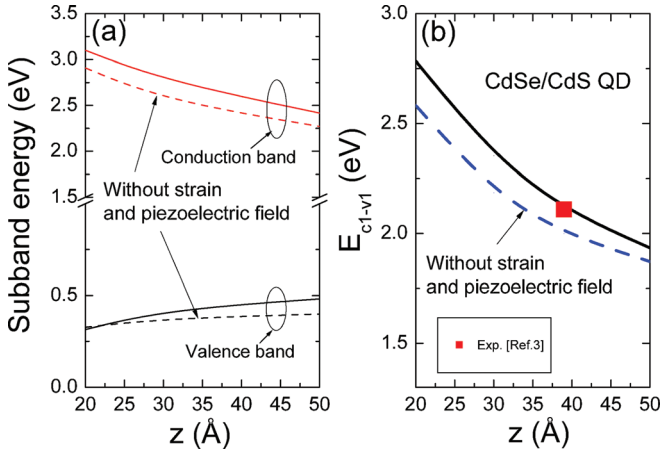

FIG. 4. (Color online) (a) Ground-state subband energies in the conduction and the valence bands and (b) interband transition energies as a function of the diameter of the CdSe QD for strained CdSe/CdS core/shell QD structures and comparison with experimental data. The experimental data for the CdSe/CdS core/shell QD structure was taken from Ref. 6. For comparison, we plotted results for subband energies without strain and piezoelectric field effects.

strain and piezoelectric field effects. Here, we used A_5 as a fitting parameter and A_6 is obtained from the relation $A_6 = 2\sqrt{2}A_5 - A_3/\sqrt{2}$.[15] Also, we used the following relations to obtain $D_{3,4,6}$: $D_3 = -(D_1 - D_2)$, $D_4 = -D_3/2.0$, and $D_6 = (D_3 + 4D_5)/\sqrt{(2.0)}$.[22] The subband energies in the conduction and the valence bands are shifted downward with the inclusion of the piezoelectric field, as shown in Fig. 1. On the other hand, the subband energies in the conduction and the valence bands are shifted upward with the inclusion of the strain effect. We know that the strain effect is larger than the piezoelectric field effect in the shift of the subband energies. As a result, interband transition energies are blueshifted with the inclusion of strain and piezoelectric field effects. We know that the theoretical interband transition energy shows a reasonable agreement with the experimental result. The interband transition energies are sensitive to the valence band effective-mass parameter A_5.

IV. SUMMARY

In summary, optical properties in CdSe/CdS core/shell quantum dots were investigated using an eight-band strain-dependent $\mathbf{k} \cdot \mathbf{p}$ Hamiltonian. The subband energies in the conduction and the valence bands were shifted downward with the inclusion of the piezoelectric field, whereas those were shifted upward with the inclusion of the strain effect. As a result, interband transition energies are blueshifted with the inclusion of strain and piezoelectric field effects because the strain effect is larger than the piezoelectric field effect in the shift of the subband energies. The theoretical interband transition energy shows a reasonable agreement with the experimental result. The piezoelectric field effect on the subband energy is negligible for QDs with small QD size.

[1]D. Bimberg, M. Grundmann and N. N. Ledentsov: Quantum Dot Heterostructure (Wiley, New York, 1999).
[2]S. Mackowski, Thin Solid Films **412**, 96 (2002).
[3]X. Peng, Acc. Chem. Res. **43**, 1387 (2010).
[4]O. Cherniavskaya, L. Chen, M. A. Islam, and L. Brus, Nano Lett. **3**, 497 (2003).
[5]E. Hao, H. Sun, Z. Zhou, J. Liu, B. Yang, and J. Shen, Chem. Mater. **11**, 3096 (1999).
[6]X. Peng, M. C. Schlamp, A. V. Kadavanich, and A. P. Alivisatos, J. Am. Chem. Soc. **119**, 7019 (1997).
[7]M. P. Halsall, J. E. Nicholls, J. J. Davies, B. Cockayne, P. J. Wright, and A. G. Cullis, Semicond. Sci. Technol. **3**, 1126 (1988).
[8]W. Langbein, M. Hetterich, M. Grun, C. Klingshirn, and H. Kalt, Appl. Phys. Lett. **65**, 2466 (1994).
[9]A. H. Nethercot, Phys. Rev. Lett. **33**, 1088 (1974).
[10]Y. W. Kwon and H. Bang, *The Finite Element Method using Matlab* (CRC Press, New York, 2000).
[11]http://www.comsol.com/.
[12]E. Berkowicz, D. Gershoni, G. Bahir, E. Lakin, D. Shilo, E. Zolotoyabko, A. C. Abare, S. P. DenBaars, and L. A. Coldren, Phys. Rev. B **61**, 10994 (2000).
[13]Y. Zhang, Phys. Rev. B **49**, 14352 (1994).
[14]T. K. Bergstresser and M. L. Cohen, Phys. Rev. **164**, 1069 (1967).
[15]J.-B. Jeon, Yu. M. Sirenko, K. W. Kim, M. A. Littlejohn, and M. A. Stroscio, Solid State Commun. **99**, 423 (1996).
[16]M. Tchounkeu, O. Briot, B. Gil, J. P. Alexis, and R.-L. Aulombard, J. Appl. Phys. **80**, 5352 (1996).
[17]B. A. Auld, *Acoustic Fields and Waves in Solids* (Wiley, New York, 1990), p.383.
[18]Landolt-Börnstein, *Group III:Condensed Matter, ser. Numerical Data and Functional Relationships in Science and Technology* (Springer, New York, 2002).
[19]O. Madelung, *Semiconductors: Data Handbook*, 3rd ed. (Springer, Berlin, 2004).
[20]K. H. Huebner, D. L. Dewhirst, D. E. Smith, and T. G. Byrom, *The Finite Element Method for Engineers*, 4th ed. (Wiley, New York, 2001).
[21]M. K. Kuo, T. R. Lin, K. B. Hong, B. T. Liao, H. T. Lee, and C. H. Yu, Semicond. Sci. Technol. **21**, 626 (2006).
[22]S. H. Park and S. L. Chuang, Phys. Rev. B **59**, 4725 (1999).